Asia-Pacific Journal of Atmospheric Sciences (2026) 62:10
https://doi.org/10.1007/s13143-025-00428-1

Online ISSN 1976-7951
Print ISSN 1976-7633

ORIGINAL ARTICLE

Identifying Major CO_2 and CH_4 Emission Sources with the STILT Model in the Seoul Metropolitan Area During Winter 2024, Including the ASIA-AQ Campaign

Hyeongseok Choi[1] · Jongbyeok Jun[1] · Yongjoo Choi[1]

Received: 6 November 2025 / Revised: 27 December 2025 / Accepted: 29 December 2025

Abstract

To investigate urban enhancements of greenhouse gases (GHGs), CO_2 and CH_4 were measured in Seoul from January to March 2024 including the Airborne and Satellite Investigation of Asian Air Quality (ASIA-AQ) campaign. Mean concentrations of both CO_2 and CH_4 exceeded those reported for other major urban cities during winter. Identified four high-concentration episodes occurred under elevated CO and low wind speeds, consistent with suppressed ventilation after long-range transport. The footprint analysis indicated that the contribution of South Korea was dominant in most episodes indicating mainly influenced by local emission sources; however, episode 4 showed a relatively larger upwind (other) contribution suggesting the long-range transport. The contribution of emission sectors indicated that buildings/heating and power generation dominated ΔCO_2 (subtracted by background concentration) variability, whereas waste management led ΔCH_4, with secondary contributions from agriculture, buildings, and fuel exploitation. Despite different major emission sectors, ΔCO_2 and ΔCH_4 converged with a narrow range with high correlation coefficient (R), reflecting co-located anthropogenic sources during wintertime. A diurnal variation of both ΔCO_2 and ΔCH_4 peaked in the morning, then reached local minimum in mid-afternoon with increasing PBL height. However, the diurnal variation of the simulated ΔCO_2 and ΔCH_4 from the Stochastic Time-Inverted Lagrangian Transport (STILT) model showed late-afternoon minimum compared to measured values because the STILT overestimates the afternoon vertical gradient of CO_2, likely owing to biases in diagnosed PBL height. This approach might provide scientific evidence to policy makers to attain the carbon neutral by suitable regulation for major emission sources when more dense spatial resolution of bottom-up inventory and meteorological fields are available.

Keywords CO_2, CH_4 · STILT model · *in-situ* measurements · ASIA-AQ

1 Introduction

Carbon dioxide (CO_2) and methane (CH_4) are the greenhouse gases (GHGs) that significantly influence global warming, and their atmospheric concentrations have substantially increased since the 1870s Industrial Revolution (Forster et al. 2007; Rigby et al. 2008). Both CO_2 and CH_4 have contributed approximately 81% of direct anthropogenic radiative forcing (Seto et al. 2014). In particular, CH_4 accounts for approximately one-third of the radiative forcing of CO_2 (Miller et al. 2013) and over a 100-year horizon its Global Warming Potential (GWP) is about 27.2 to 29.8 times that of CO_2 (Masson-Delmotte et al. 2021).

Both long-lived GHGs are particularly critical for stabilizing the climate, because a substantial fraction of anthropogenic CO_2 emissions remain in the atmosphere for centuries to millennia (Parry 2007; Stocker et al. 2013). The emissions of CO_2 and CH_4 from anthropogenic sources are jointly responsible for the dominant share of current and projected future climate warming (Allan et al. 2023). To achieve the long-term temperature goals of the Paris Agreement, Parties communicate Nationally Determined Contributions (NDCs) every five years and

✉ Yongjoo Choi
choingjoo@hufs.ac.kr

[1] Department of Environmental Science, Hankuk University of Foreign Studies, Yongin, Gyeonggi 17035, Republic of Korea

Published online: 02 February 2026

evaluate collective progress through the Global Stocktake (GST) (UNFCCC 2015). Under the Paris Agreement's Enhanced Transparency Framework, Measurement, Reporting, and Verification (MRV) is fundamental to this process by ensuring the availability and scientific robustness of GHGs information. Measurement provides the empirical basis for evaluating NDC implementation and strengthening the credibility of the GST. Accordingly, accurate in-situ observations and sustained monitoring are essential for supporting effective climate mitigation assessment. Therefore, understanding the detailed behaviors of GHGs from *in-situ* measurements is required to establish the mitigation policies to achieve the carbon neutral by mid-century.

Global background monitoring by the National Oceanic and Atmospheric Administration Global Monitoring Laboratory (NOAA/GML) indicates that atmospheric concentrations of CO_2 and CH_4 have already risen to 422.8 ppm and 1,929.9 ppb, respectively, in 2024 (Lan et al. 2025a; b). Among the contributors to increasing CO_2 on a global scale, East Asia makes a particularly critical contribution, accounting for 35% (18.6 Gt CO_2-eq) of global emissions (Crippa et al. 2024). For instance, annual mean concentrations in Shanghai from June 2017 to May 2018 were 428.36 ppm for CO_2 and 2,154 ppb for CH_4 (Wei et al. 2020). Correspondingly, elevated levels have been observed in Seoul, where the mean CO_2 concentration from July to December 2019 reached 451.76 ppm (Park et al. 2021).

Several studies have examined the sources and origins of GHGs in Korea, primarily employing measurements from background monitoring sites such as Anmyeon-do (AMY), a World Meteorological Organization (WMO) Global Atmosphere Watch (GAW) station (Kim et al. 2023; Lee et al. 2020; Li et al. 2024; Sim et al. 2022). Background sites such as AMY provide valuable insights into regional and long-range transport (Lee et al. 2019), whereas they are less suited to capturing the complex emission characteristics of densely populated metropolitan areas. In contrast, urban areas account for nearly 70% of global CO_2 emissions from energy use (Seto et al. 2014), indicating the importance of central cities in global anthropogenic GHGs emissions. Urban areas are major hotspots of anthropogenic emissions, where fossil fuel combustion, traffic, industrial activities, and residential heating interact in ways that differ substantially from background conditions. Despite these reasons, a research explicitly targeting Seoul remains scarce, particularly in terms of source attribution and quantitative assessments of sectoral contributions. This deficiency emphasizes the urgent need for studies that integrate high-resolution modeling with *in-situ* measurements to better constrain GHG emissions in Korea's most densely populated metropolitan region.

The Airborne and Satellite Investigation of Asian Air Quality (ASIA-AQ) campaign was conducted from February to March 2024 as a large-scale international collaboration by NASA, many universities, and environmental agencies from South Korea, the Philippines, Thailand, and Taiwan (Crawford et al. 2022). The objective of the campaign was to improve understanding of atmospheric composition and GHG distributions across Asia by combining airborne, satellite, and ground-based measurements. Accordingly, this study investigates the temporal variability and source characteristics of atmospheric CO_2 and CH_4 in Seoul from January to March 2024 including the ASIA-AQ campaign. *In-situ* measurements were integrated with model simulations using the Stochastic Time-Inverted Lagrangian Transport (STILT) model driven by Global Forecast System (GFS) meteorological data provided by the National Centers for Environmental Prediction (NCEP, NOAA) and sectoral emission rates from the Emissions Database for Global Atmospheric Research (EDGAR) inventory. Measured and simulated CO_2 and CH_4 concentrations were analyzed to examine their temporal variation, the enhancement ratios between CH_4 and CO_2 ($\Delta CH_4/\Delta CO_2$), and diurnal variations to identify their behaviors and contributions of region and emission sectors.

2 Methods

2.1 Measurement Site and Period

This study was conducted on the 7th floor of the Mediheal Environmental Science Building (37.59°N, 127.03°E, 72 m a.s.l.) at Korea University in Seongbuk-gu, Seoul, Korea from 28 January to 28 March including ASIA-AQ campaign (Fig. 1). The emissions of Seoul are significantly influenced by anthropogenic activities such as transportation, industrial operations, and commercial activities. It should be noted that the impact of biospheric CO_2 uptake is minimal due to low photosynthetic activity, while anthropogenic emissions are dominant (Bezyk et al. 2023) because the measurements were conducted during wintertime. In contrast, CH_4 uptake exhibited a general decrease, attributable to variations in soil moisture and temperature (Bezyk et al. 2022). Furthermore, given the considerable atmospheric lifetimes of CO_2 and CH_4, the site is influenced by not only the local emission but also long-range transport from mainland including China, North Korea.

2.2 Instrument

We utilized a GHG analyzer (model GLA331-GGA; ABB-LGR Inc.), equipped with a high-precision measurement

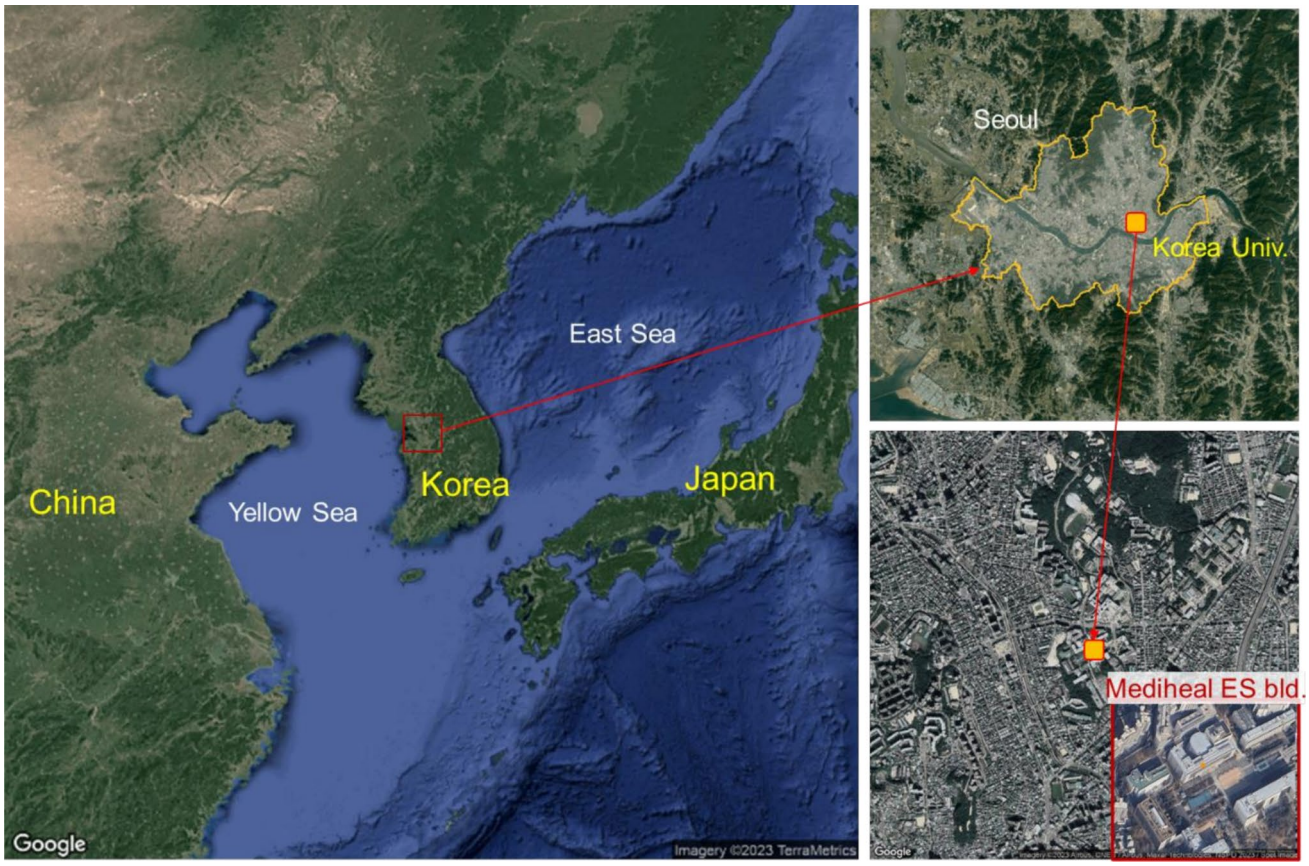

Fig. 1 Locations of the measurement site (37.59°N, 127.03°E, 72 m a.s.l.; Mediheal Environmental Science Building in Korea University, Seoul, Korea). The left panel shows map of East Asia including, China, Korea, and Japan

system based on Off-Axis Integrated Cavity Output Spectroscopy (OA-ICOS), a highly sensitive and widely used technology for trace gas monitoring (Paul et al. 2001). This technique operates on the principle of directing a laser beam into an optical cavity at an off-axis angle, resulting in multiple reflections between highly reflective mirrors. Such a configuration eliminates the stringent alignment stability and laser wavelength locking requirements of conventional resonance-based optical techniques, while maintaining an extremely long effective optical path length (on the order of several kilometers), thereby enabling ultra-sensitive detection and high-precision measurements (Baer et al. 2002). Measurements were conducted at a sampling frequency of 1 Hz. The analyzer provides high precision, with accuracies of ± 0.15 ppm for CO_2 and ± 0.6 ppb for CH_4. The measurement ranges spanned from 0 to 200,000 ppm for CO_2 and 0 to 100 ppm for CH_4, allowing effective detection of a wide range of concentration variability commonly observed in urban environments.

CO_2 and CH_4 concentrations were calibrated to the WMO X2019 (Hall et al. 2021) and X2004A (Dlugokencky et al. 2005) mole fraction standard scales, respectively, provided by NOAA/GML, which serves as the WMO Central Calibration Laboratory (CCL) for WMO/GAW. Ambient air was continuously drawn into the analyzer, enabling real-time detection of short-term fluctuations in atmospheric GHG concentrations.

To quantitatively assess the local contributions of urban GHG emissions, ΔCO_2 and ΔCH_4 (i.e., enhancements above the background level) were calculated by subtracting the baseline level from the observed CO_2 and CH_4 mixing ratios. The baseline, representing atmospheric conditions minimally influenced by local urban emissions, was estimated using a 14-day moving 5th percentile (Ammoura et al. 2016; Choi et al. 2020).

2.3 STILT Model Configuration

We utilized the STILT model version 2 (Fasoli et al. 2018), which is a widely used Lagrangian atmospheric transport model. This model simulates backward trajectories of air parcels arriving at the receptor site, deriving footprints that represent the sensitivity of an observation to surface fluxes from upwind regions (Lin et al. 2003), enabling the identification of potential source regions and the separation of local emissions from long-range transport influences

such as those from northeastern and eastern China. Prior to running the STILT model, it is essential to select appropriate meteorological fields. While most previous studies adopt the Weather Research and Forecasting (WRF) model coupled with the STILT (WRF-STILT), providing high-resolution meteorological fields (Kort et al. 2013; Maier et al. 2021; Nehrkorn et al. 2010; Park et al. 2022), we used GFS with a 0.25° resolution. In this study, we configured the model to release 1,000 virtual particles at the receptor (measurement) site. The backward trajectories of these particles were simulated at 1-h intervals, extending up to 5 d prior to the arrival time, allowing us to identify the origin of emissions and assess transport mechanisms influencing the SMA. Our footprints were generated at a spatial resolution of 0.1° by 0.1°.

Figure 3 shows the footprint distribution from the STILT model during the measurement period. Since footprints indicate the sensitivity of the receptor to surface fluxes, high sensitivity is observed over the Korean peninsula near the measurement site. Furthermore, transport pathways from northeastern and eastern China are also clearly identified.

2.4 CO_2 and CH_4 Emission Inventory

CO_2 and CH_4 enhancements were estimated by convolving footprints with gridded surface fluxes from the Emissions Dataset for Global Atmospheric Research GHG (EDGAR_2024_GHG; https://edgar.jrc.ec.europa.eu/dataset_ghg2024) for CO_2 and CH_4 based on 2024, a bottom-up global anthropogenic GHGs emission inventory. In addition to anthropogenic sources, biomass burning emissions were considered using the Global Fire Assimilation System (GFAS) v1.2 (https://www.ecmwf.int/en/forecasts/dataset/global-fire-assimilation-system), which provides wildfire fluxes of CO_2 and CH_4. These datasets provide a spatial resolution of 0.1° by 0.1°, while the temporal resolutions are 1 month for EDGAR and 1 day for GFAS, respectively. Simulated CO_2 and CH_4 concentration contributions from individual emission sectors can be calculated using Eq. (1),

$$GHG_{simulated} = \sum_{i=1}^{n} (footprint \times ER_i) \quad (1)$$

where $GHG_{simulated}$ denotes the simulated CO_2 or CH_4 concentration; footprint is the STILT simulated influence-weighted functions (units: ppm·m^2 ·s·mol^{-1}), *ER* is the sector-specific emission rate of CO_2 and CH_4 in each grid cell (units: mol m^{-2} ·s^{-1}), *n* is the number of all sectors in bottom-up emission inventories (Fig. 2). The simulated concentrations were compared with *in-situ* measurements to evaluate regional and sectoral contributions.

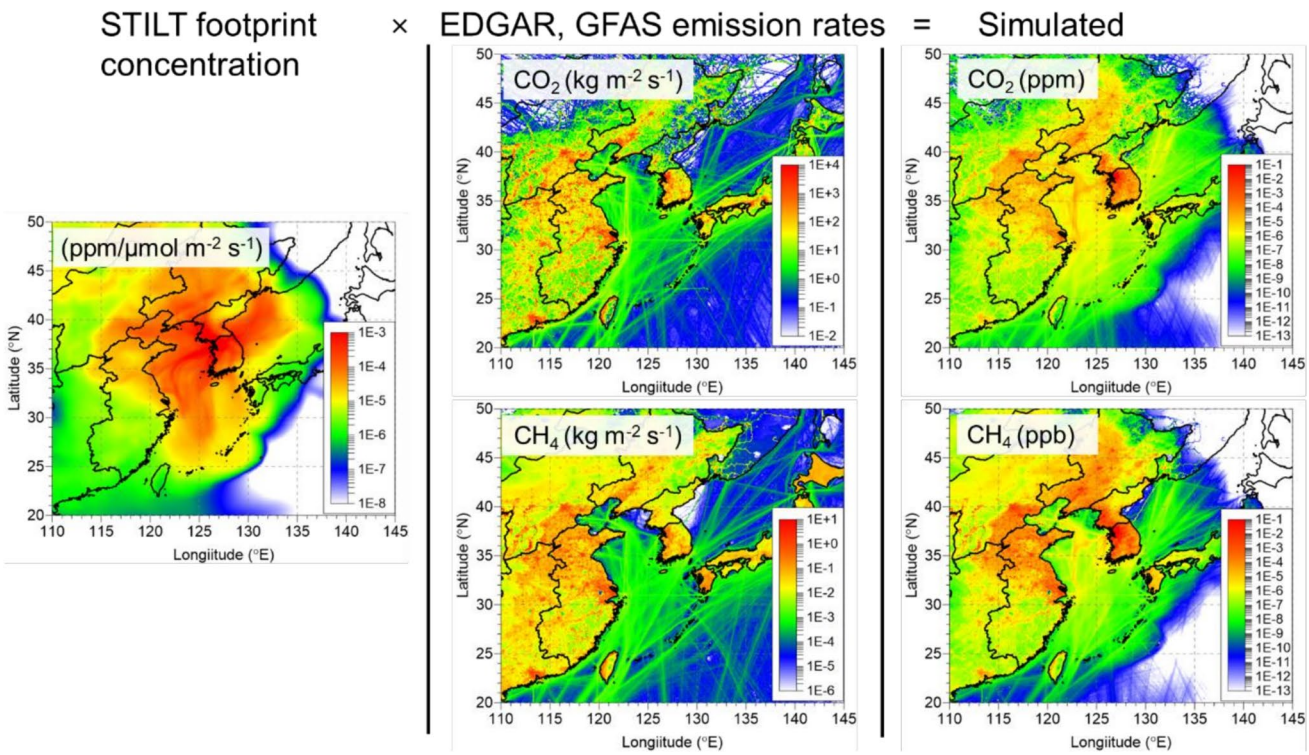

Fig. 2 The averaged footprints calculated from the Stochastic Time-Inverted Lagrangian Transport (STILT) model (left), total emission rates of CO_2 and CH_4 from Emissions Dataset for Global Atmospheric Research (EDGAR) emission inventories and Global Fire Assimilation System (GFAS) v1.2, and simulated concentratoin of CO_2 and CH_4 by multiplying the footprint by emssion rates

3 Results

3.1 Time Series of CO_2 and CH_4

Figure 3 depicts observed hourly CO_2 and CH_4 concentrations, along with the major contributing countries indicated by vertical bars. The observed mean concentrations were 465 ± 20.5 ppm for CO_2 and 2,203 ± 86.8 ppb for CH_4 during the measurement period. These concentrations are notably higher than Wroclaw in Poland (433 ppm for CO_2 and 2,010 ppb for CH_4; Bezyk et al. 2023), Shadnagar in India (395.94 ± 1.02 ppm for CO_2 and 1,950 ± 10 ppb for CH_4; Sreenivas et al. 2022), and Shanghai in China (435.49 ppm for CO_2 and 2,140 ppb for CH_4; Wei et al. 2020) during winter. In addition, the SMA mean concentrations were consistently higher than those observed at background sites in South Korea (Anmyeon-do, Ulleung-do and Gosan), where wintertime CO_2 and CH_4 levels ranged from 430–434 ppm and 2,033–2,050 ppb, respectively, indicating substantial urban enhancements within the SMA (KMA 2025). This is consistent with the maximum concentration of CO_2 occurring during winter due to domestic heating and the stable surface layer, reduced convective mixing, and limited vegetation carbon uptake (Cheng et al. 2018). CH_4 also shows a similar seasonal pattern to CO_2, with a maximum in October and a minimum in March and April with a relatively large seasonal amplitude due to complex mechanism including strong reaction with hydroxyl radicals (OH) in summer and seasonal variation in diverse emission sources (Kenea et al. 2021).

Because daily variation in CO_2 and CH_4 are largely controlled by the regional distribution of emission sources and atmospheric transport at the synoptic scale (Sreenivas et al. 2022), we selected high concentration episodes for which daily average CO_2 concentrations exceeded 460 ppm (~median). Although the daily average might be lower than the threshold, if concentrations above the threshold persisted for a short period, it was deemed reasonable to treat the period as a single event. Therefore, high concentration episodes were defined as periods with an average concentration exceeding 480 ppm (~75% percentile). The start and end dates of each episode were chosen based on whether the CO_2 concentration was above or below 460 ppm. This ensured that days with lower concentrations following a high-concentration peak could still be included in the episode, and captured the rise in concentrations from the time

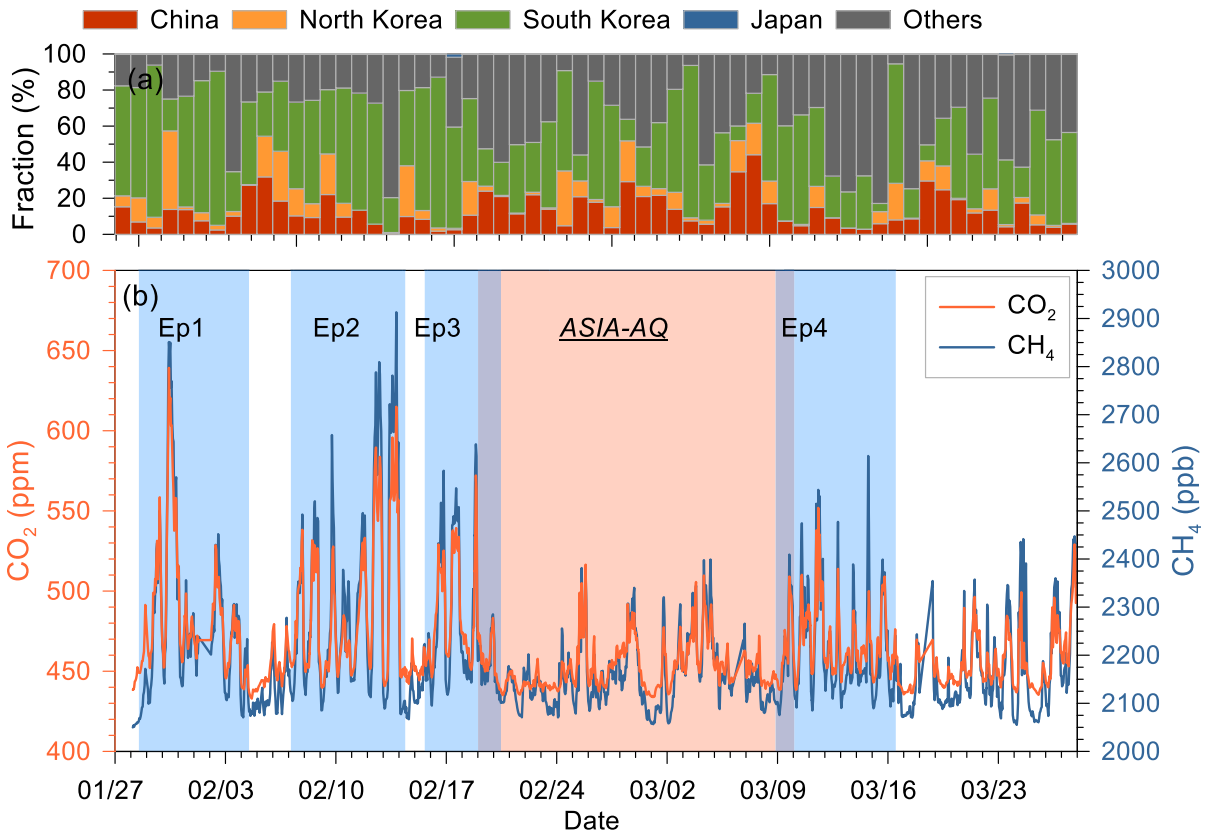

Fig. 3 Temporal variations in regional contribution and concentration of CO_2 and CH_4. Top panel: fractional of regional contribution calculated from the STILT model over selected area (red –China; orange –North Korea; green – South Korea; blue – Japan; grey –other regions such as the ocean). Bottom panel: measured concentrations of CO_2 and CH_4. The periods denoted as Ep1–4, and ASIA-AQ campaign periods (see the text for details) are enclosed by shaded box with blue and pink, respectively

they first exceeded 480 ppm at the beginning of the episode. According to the criteria, we selected four high concentration cases of CO_2 and CH_4 during the measurement period (30–31 January, 12–14 February, 16–20 February, and 28 March 2024). It should be noted that high CH_4 concentrations were assigned to the same CO_2 episodes because the hourly variation showed good consistency between CO_2 and CH_4.

3.2 High CO_2 and CH_4 Concentration Episodes

Table 1 summarizes the mean values of measured CO_2 and CH_4 concentrations along with meteorological variables and air pollutants from the Air Quality Monitoring Station (AQMS), which is located 1.1 km from the measurement site. CO_2 and CH_4 concentrations during the episodes were elevated by approximately 11–36 ppm and 42–147 ppb, respectively, compared to non-event days. During the high concentration episodes, atmospheric pollutant concentrations also increased, particularly CO, a tracer of long-range transport, which showed an increase of up to 76% during episode (Ep) 2. In urban environments, however, CO can also be influenced by local emissions (e.g., traffic emissions). Accordingly, we examined diagnostic ratios among air pollutants (CO/NO_2 and O_3/NO_2) to evaluate the relative influence of local emissions and long-range transport. Ep1 and Ep3 exhibited relatively lower CO/NO_2 and O_3/NO_2 than all periods and non-event periods, suggesting a higher fraction of short-lived NO_2 and limited photochemical processing. This pattern is more consistent with a stronger influence of local emissions. In contrast, Ep2 was characterized by elevated CO and $PM_{2.5}$ along with a relatively higher CO/NO_2, supporting a greater contribution from transported pollution (Shim et al. 2019). Ep4 showed comparatively lower CO and $PM_{2.5}$, indicating weaker pollution accumulation than Ep1–Ep3. Additionally, it also exhibited a higher O_3/NO_2 ratio (1.2), along with higher wind speeds. The ground meteorological variables did not show a significant difference between episodes and non-event days except for wind speed; the wind speeds on non-event days were higher than those during episodes, indicating that ventilation is one of the key factors driving lower concentrations of CO_2, CH_4, and air pollutants ($R = -0.93$ for CO_2 and -0.82 for CH_4). Kim et al. (2015) demonstrated using satellite observations that a high concentration of CO_2 plume could be long-range transported with 1–2 day duration.

To investigate the regional contribution, we calculated the fractions of residence time based on the footprints simulated from the STILT model (Fig. 3a). Except for Ep4, the averaged contribution of South Korea accounted for more than 50%, followed by others (~28%), China (~9.3%), and/or North Korea (8.0%), and Japan (0.2%) during the episodes (Table 1). This implied that local emissions from South Korea (mainly from the Seoul Metropolitan Area) might be lead the elevated CO_2 and CH_4 concentrations compared to long-range transport from North Korea, China, and other regions. However, Ep4 exhibited a different pattern with South Korea contributing 36.7%, followed by others (51.2%), China (8.2%), North Korea (4.0%). This pattern indicated transported CO_2 and CH_4 might be more pronounced under relatively higher wind speeds observed in Ep4, similar to non-event conditions.

Table 1 Summaries of selected periods for CO_2 and CH_4, atmospheric pollutants, meteorological paramaters, and regional contributions measured in Seoul, Korea

	All	Ep1	Ep2	Ep3	Ep4	Non-event
CO_2 (ppm)	465±29.8	491±41.5	486±38.3	482±30.4	466±21.6	455±21.0
CH_4 (ppb)	2,204±135.4	2,287±177.0	2,312±179.9	2,266±142.5	2,207±108.6	2,165±101.0
$PM_{2.5}$	22.1±16.2	35.3±18.5	39.5±14.8	20.6±12.7	24.4±9.0	17.0±14.0
SO_2	2.55±0.62	3.43±0.56	2.90±0.48	2.63±0.44	2.63±0.58	2.32±0.50
CO	523±216.2	746±259.5	775±276.9	623±183.1	504±106.8	440±144.0
O_3	28±14.1	19±14.3	26±17.5	14±10.6	33±15.8	30±11.8
NO_2	25.5±15.3	39.9±17.1	34.2±20.8	33.9±12.5	27.2±13.7	20.6±11.6
Temp	5.42±4.6	3.11±3.3	3.34±3.9	6.04±3.7	6.70±3.6	5.82±4.9
WS	1.72±1.0	1.25±0.7	1.47±1.0	1.34±0.6	1.65±1.0	1.89±1.1
RH	58.0±18.9	55.0±13.5	59.6±12.5	75.5±17.5	53.3±16.7	57.2±19.9
CO/NO_2	20.5	18.7	22.7	18.4	18.5	21.4
O_3/NO_2	1.1	0.5	0.8	0.4	1.2	1.5
Regional contribution						
South Korea	43.1±21.2	57.9±25.7	50.9±16.5	54.9±21.2	36.7±19.1	38.2±18.7
China	13.2±9.11	8.28±4.18	10.1±6.12	9.44±7.99	8.20±4.89	16.6±9.82
North Korea	7.88±9.35	10.6±14.0	7.59±8.00	5.78±6.58	3.96±5.17	8.62±9.19
Japan	0.06±0.25	0.00±0.00	0.02±0.03	0.45±0.70	0.00±0.00	0.05±0.11
Others	35.8±20.2	23.3±18.3	31.4±19.9	29.4±14.3	51.2±24.1	36.6±17.8

3.3 Source Contribution of ΔCO_2 and ΔCH_4 Concentrations

Figure 4 shows the time-series of simulated ΔCO_2 and ΔCH_4 concentrations depending on the emission sectors from EDGAR inventories with GFAS data. During the measurement period, the sum of simulated sectoral concentrations showed good correlation with measured ΔCO_2 ($CO_{2,\ observed} - CO_{2,\ background}$) with high correlation coefficients ($R > 0.63$) and slope of best-fit lines close to unity (> 0.83). The statistics were comparable to previous studies (Kenea et al. 2023; Sreenivas et al. 2016, 2022; Tohjima et al. 2014; Xia et al. 2020). The discrepancy between simulated and measured concentrations might be caused by the uncertainty in input parameters such as emission factors in sectoral emission rates (Solazzo et al. 2021), meteorological fields, imprecise assumed background CO_2 and/or CH_4 concentrations, uncertainties in the STILT transport modeling framework (Yang et al. 2025). Although the emission from biomass burning were included in Fig. 4, it should be noted that this study mainly focused on anthropogenic emissions by considering the EDGAR inventories and subtracting background concentration from the measured values. In other words, natural sources (e.g., CO_2 from ecosystem respiration and CH_4 from wetlands) were not explicitly accounted for, even though winter photosynthesis is reduced for CO_2.

The daily variation of emission sectors for ΔCO_2 was mainly derived by the buildings (21.1 ppm) and power generation (12.2 ppm), followed by transportation (3.8 ppm) and industry (2.11 ppm). The remaining sectors (fuel exploitation, waste, agriculture) were negligible due to their low concentration (less than 0.39 ppm). Therefore, the R between dominant sectors and measured ΔCO_2 exceeded 0.55. In EDGAR, the buildings sector includes small-scale combustion emissions from residential and commercial heating, with spatial allocation informed by population

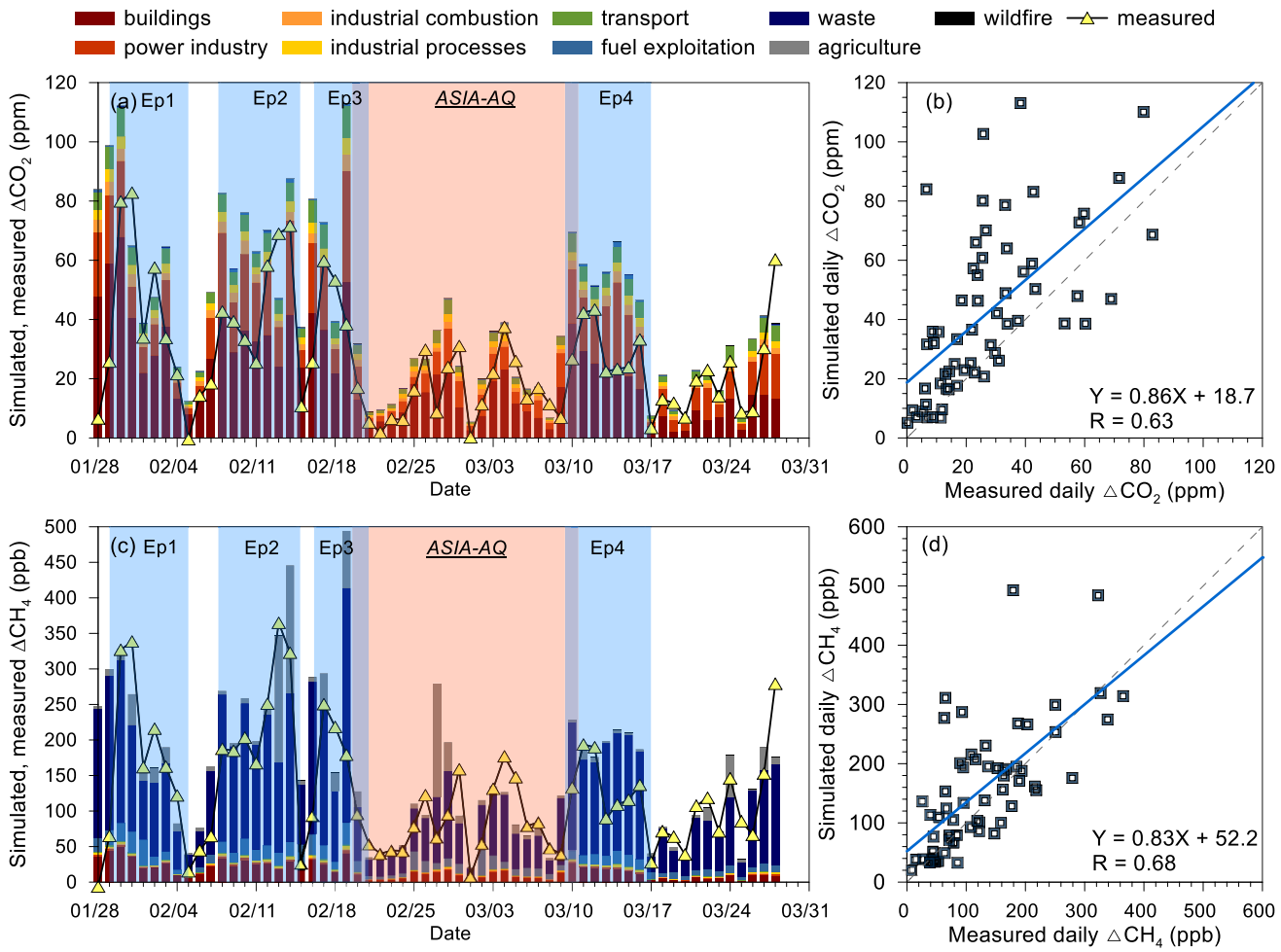

Fig. 4 Daily variations in simulated concentration of emission sectors and measured concentrations of (**a**) ΔCO_2 and (**c**) ΔCH_4. The periods denoted as Ep1–4, and ASIA-AQ campaign periods (see the text for details) are enclosed by shaded box with blue and pink, respectively. (**b**) and (**d**) show the scatter plots between the sum of simulated and measured concentrations. The solid blue and dashed-black indicate best-fit and 1:1 lines, respectively

density and heating degree-days to represent regional variability in heating demand (Crippa et al. 2024).

For ΔCH_4, the major emission sector was identified as waste (106 ppb) with an overwhelming contribution compared to others, resulting in high R (0.55) with ΔCH_4. This is consistent with previous evidence that waste is a major methane emission source in Korea (Moon et al. 2024). The remaining moderately contributing sectors, such as agriculture (19.8 ppb), buildings (16.4 ppb), and fuel exploitation (13.9 ppb) also showed similar R levels (0.34–0.51) with ΔCH_4. These moderate contributions might be reflected in the limited agricultural activity and temperature-dependent emissions during winter. Although ΔCO_2 and ΔCH_4 showed similar temporal trends, their leading emission sources differed, indicating that distinct sectoral processes can yield convergent daily patterns under specific urban and seasonal settings.

Figure 5 presents sectoral concentrations and contributions during episodes and non-event days. Aforementioned, the buildings and power sectors dominated ΔCO_2 both in concentration and contribution. For most sectors, simulated ΔCO_2 concentrations were roughly twice those on non-event days, with the exception of agriculture and wildfire. Despite this increase, sectoral shares remained broadly similar between episodes and non-event days. Ep4, which showed a notable contribution from the "other" region, also exhibited a higher fraction from power generation than other episodes, suggesting influence from long-range transport of power-plant emissions. ΔCH_4 shows a similar pattern; the simulated concentrations for most sectors were about twice those of non-event days, except for wildfire. During Ep4, the power generation, industrial processes, and waste sectors made comparatively larger contributions, suggesting influence from upwind industrial and waste CH_4 sources (e.g., industrial wastewater) (Chen et al. 2025).

3.4 The Relationship Between ΔCO_2 and ΔCH_4

ΔCO_2 and ΔCH_4 exhibited remarkably similar variation patterns, indicating that both GHGs are primarily influenced by similar controlling factors, such as anthropogenic emission sources, boundary layer dynamics, and/or regional

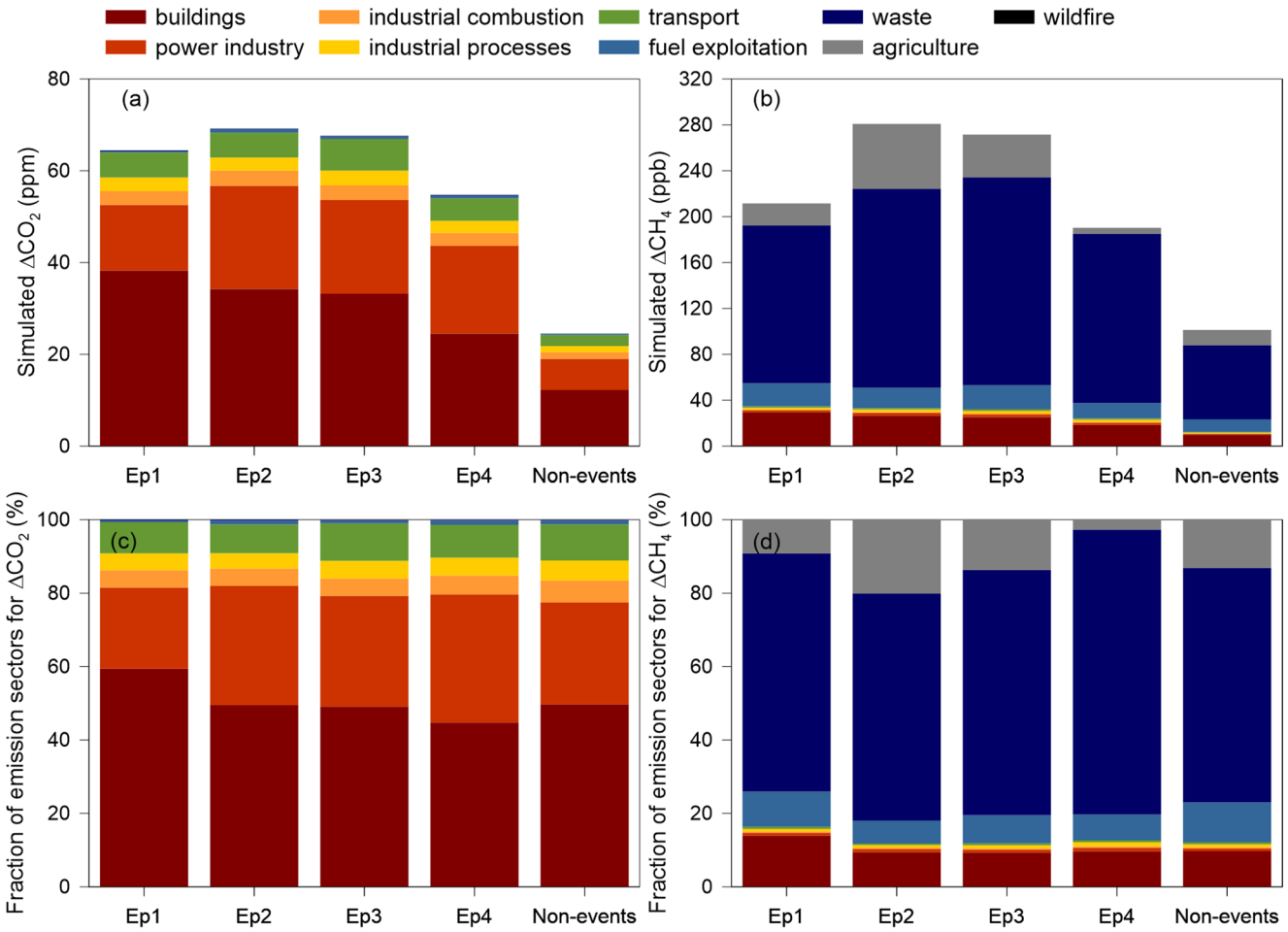

Fig. 5 The simulated sectoral concentrations and fractional contributions to the total simulated concentrations of ΔCO_2 (top) and ΔCH_4 (bottom) during the episodes and on non-event days

transport patterns by sharing similar spatiotemporal drivers in this study region. $\Delta CH_4/\Delta CO_2$ ratio serves as an effective indicator for monitoring regional emission variations and estimating the relative contribution from different emission sources (Chandra et al. 2019; Kenea et al. 2023; Sreenivas et al. 2022; Tohjima et al. 2014). During the measurement period, the slope of best-fit line between ΔCH_4 and ΔCO_2 ratio was 4.56 ppb ppm^{-1} with a convergence within a narrow range (R = 0.96) (Fig. 6). The positive slope could be explained by a minimal CO_2 and CH_4 sinks due to oxidation by OH in winter (Chandra et al. 2022; Sreenivas et al. 2022). It should be noted that R values between ΔCH_4 and ΔCO_2 from previous studies were much lower compared to our results (0.77 for Shadnagar, 0.78 for Hateruma Island, and 0.73 for Anmyeon-do). Whereas the strong correlation (R > 0.8) between ΔCO_2 and ΔCH_4 suggests similar controlling emission processes at the site. Therefore, CH_4 and CO_2 emissions in this study region are highly related to anthropogenic emission sources such as natural gas combustion near the measurement site.

The $\Delta CH_4/\Delta CO_2$ ratio from this study was ranked lower range compared to those from Anmyeon-do (5.6 ppb ppm^{-1} during 2010–2020), background area in Korea (Kenea et al. 2023), Hateruma Island (~10 ppb ppm^{-1} in 2010), background area in Japan (Tohjima et al. 2014), Shadnagar (7.1 ppb ppm^{-1} in 2014 and 9.40 ppb ppm^{-1} during 2014–2017) at a suburban site in India (Sreenivas et al. 2016, 2022) during wintertime. However, the ratio from Jingdezhen (3.92 ppb ppm^{-1}), semi-urban region in China (Xia et al. 2020) was slightly lower than our results. Because the change in slope of $\Delta CH_4/\Delta CO_2$ is sensitive to the variability of atmospheric CO_2 (Sreenivas et al. 2022; Tohjima et al. 2014), the relatively high slope indicates a significant influence of ΔCO_2 over the SMA during wintertime. Park et al. (2022) reported the highest slopes in the western (10.33 ± 4.55 ppb ppm^{-1}) and eastern (14.50 ± 1.91 ppb ppm^{-1}) Seoul by discovering unveil unexpected urban CH_4 hotspots such as emission/leakage from supply of LNG and large commercial multicomplex buildings around Seoul.

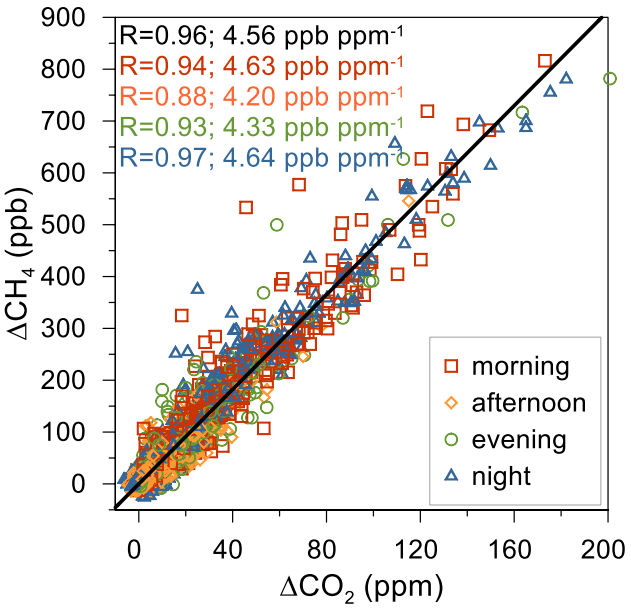

Fig. 6 Scatter plot of between ΔCH_4 and ΔCO_2 in ppb ppm^{-1} for different time windows: morning (0600–1000 h), afternoon (1100–1700 h), evening (1800–2200 h), night (0000–0500 h). The robust linear regression fit is used to obtain the ratios. Correlation coefficients (R) are also reported alongside the ratios

During the nighttime window, a strong and positive correlation was observed with maximum R value of about 0.9 resulted from fugitive emissions from natural gas infrastructure (Nara et al. 2014). By contrast, the afternoon time window showed a weak correlation, suggesting specific source/sink activities of CO_2 and CH_4, such as CH_4 loss by OH and CO_2 uptake by photosynthesis (Sreenivas et al. 2022). Several major CH_4 sources active during the daytime (such as traffic) become less prominent at night; however, fugitive CH_4 emissions occur continuously throughout the day, and their detection is enhanced at night under lower wind speeds, which reduce the atmospheric dispersion of locally emitted gases (Chandra et al. 2019).

3.5 Diurnal Variation of Anthropogenic ΔCO_2 and ΔCH_4

The diurnal variation of ΔCO_2 and ΔCH_4 exhibited remarkably similar variation patterns, indicating that both GHGs are primarily influenced by anthropogenic emission sources as mentioned in Section 3.2 (Fig. 7). The two GHG concentrations peaked at 8:00 local time (LT) for ΔCO_2 (46.0 ppm) and 10:00 LT for ΔCH_4 (217.6 ppb). These elevated concentrations are likely associated with increased anthropogenic activities such as rush hour traffic and heating for CO_2 and waste treatment for CH_4 during working hours. In contrast, the concentrations of both GHGs decreased steadily throughout the day, reaching their lowest levels in the afternoon, at 15:00 LT (11.0 ppm for ΔCO_2 and 44.2 ppb for ΔCH_4). This reduction is primarily attributed to enhanced vertical mixing in the atmosphere during the daytime, as the planetary boundary layer (PBL) typically becomes higher under strong solar irradiation (Choi et al. 2021; Soleimanpour et al. 2023), thereby promoting greater vertical dispersion and dilution of near-surface emissions. The nighttime enhancement of ΔCO_2 and ΔCH_4 concentrations is also likely driven by PBL processes and regional-scale transport (Callewaert et al. 2022). Although the diurnal variation of ΔCO_2 and ΔCH_4 shows a similar pattern with a local minimum and a second peak at nighttime, there is a time lag in the morning peak times for ΔCO_2 and ΔCH_4. The lag likely reflects

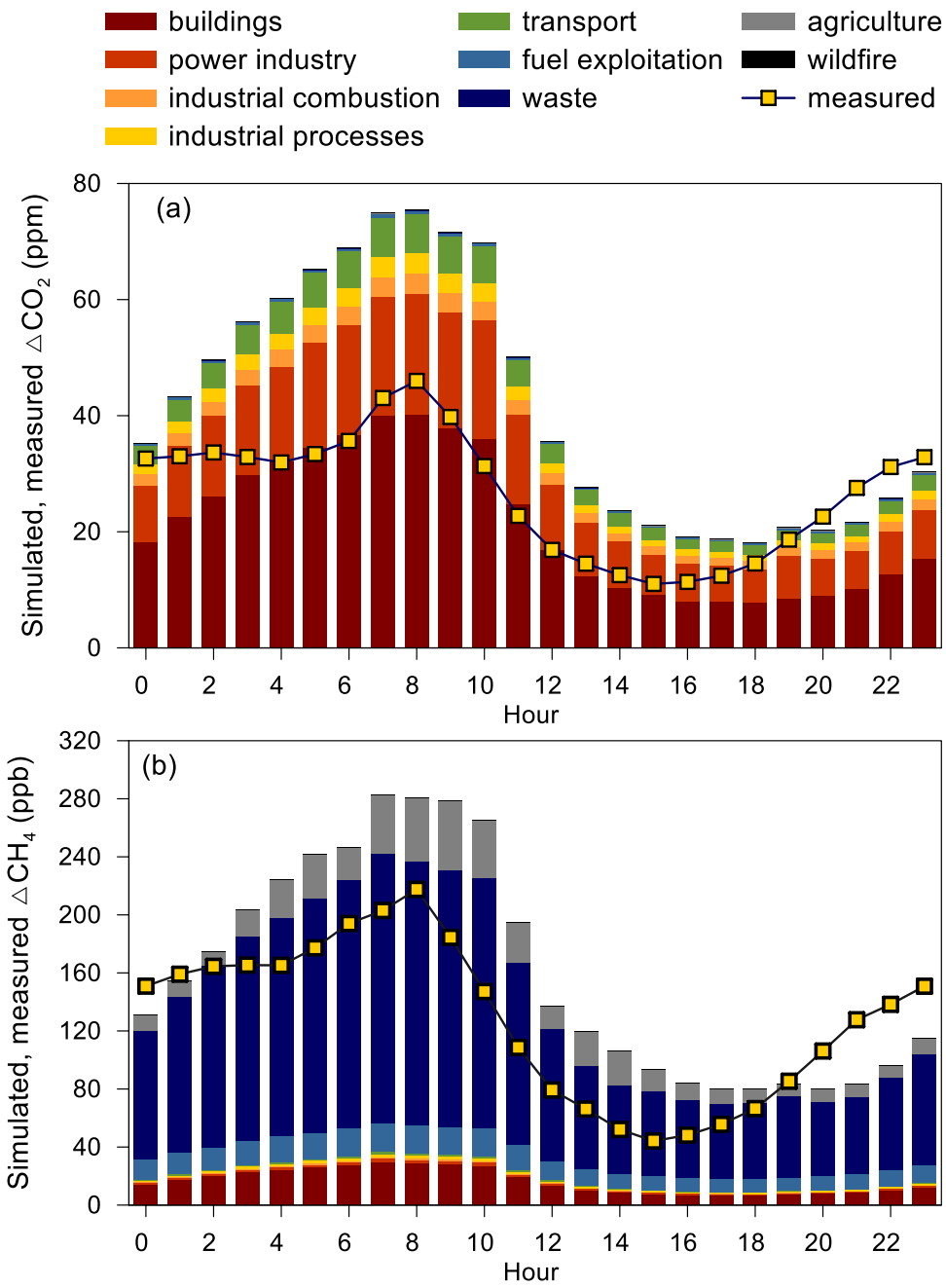

Fig. 7 Diurnal variation of simulated sectoral concentrations and measured (**a**) ΔCO_2 and (**b**) ΔCH_4

differing activity schedules of dominant sources such as heating/traffic for ΔCO_2 and waste treatment for ΔCH_4. Given that EDGAR provides monthly emission rates, the simulated CO_2 and CH_4 are limited in representing day-to-day and diurnal variability due to roughly calculated hourly emission rates from monthly-based. Moreover, the simulated diurnal sectoral contributions should be interpreted primarily as changes in footprint sensitivity driven by meteorology and transport rather than the diurnal variation of emission rate.

The coefficient of variation (CV; standard deviation divided by mean) of simulated ΔCO_2 concentration shows higher values in buildings (0.57), followed by transportation (0.50), and power generation (0.45) indicating these sectors are the main drivers of the ΔCO_2 diurnal variation. In the case of simulated ΔCH_4, the emission sectors of agriculture (0.63), buildings (0.51), and waste treatment (0.48) were identified for high diurnal variation. It should be noted that the peak and local minimum for simulated concentrations showed slightly different patterns with measured values. The simulated concentrations peaked at 08:00 LT for ΔCO_2 (75.5 ppm) and 07:00 LT for ΔCH_4 (282.5 ppb) along with local minimum at 18:00 LT for both ΔCO_2 (18.2 ppm) and ΔCH_4 (80.3 ppb).

A similar simulated diurnal pattern was reported in which both CO_2 and CH_4 peaked around 06:00 UTC and exhibited a secondary increase after 18:00 UTC in London, U.K., based on the CHIMERE model simulations (Boon et al. 2016). McKain et al. (2012) also found that simulated CO_2 concentrations peaked around 07:00 MST and increased again after 18:00 MST from the WRF–STILT simulations in Salt Lake City, U.S. For CH_4, the WRF–STILT simulated unstably elevated morning concentrations between 06:00 and 12:00 UTC, followed by a steady decrease until about 19:00 UTC during the winter of 2012–2013 at Boston, U.S. (McKain et al. 2015). It might be caused by inaccurate PBL height estimates in the STILT, which tend to yield a larger afternoon vertical gradient in GHGs concentrations than measured values (Sargent et al. 2018). Thus, updating PBL height estimation algorithms based on *in-situ* measurements should improve simulation of GHGs diurnal cycles and thereby enhance our understanding of urban GHGs behavior.

4 Conclusions

To investigate urban enhancements of greenhouse gases (GHGs), CO_2 and CH_4 were measured in the Seoul Metropolitan Area (SMA) from January to March 2024 including the ASIA-AQ campaign. The mean concentrations reached 465 ± 20.5 ppm for CO_2 and 2,203 ± 86.8 ppb for CH_4, exceeding GHGs in wintertime levels reported for other major cities, including Wroclaw, Poland, Shadnagar, India, and Shanghai, China. We identified four high concentration episodes during which CO_2 and CH_4 increased by 13.7–36.3 ppm and 53.1–169 ppb, respectively, relative to non-event days. These episodes co-occurred with elevated CO and reduced wind speeds, indicating suppressed ventilation and episodic regional transport. The contribution of South Korea was pronounced in episodes 1–3, consistent with dominant local influences from the SMA. However, episode 4 showed a larger upwind ("other") contribution under relatively higher winds, suggesting enhanced long-range transport.

The contribution of emission sectors (EDGAR with GFAS) indicated that buildings/heating and power generation dominated CO_2 variability (~21.1 and 12.2 ppm, respectively), whereas waste management led CH_4 (~106 ppb), with secondary contributions from agriculture, buildings, and fuel exploitation. Despite different major emission sectors, ΔCO_2 and ΔCH_4 converged with narrow range, with for best-fit slope of 4.56 ppb ppm^{-1} and correlation coefficient (R) of 0.96, reflecting co-located anthropogenic sources during wintertime when biospheric and OH sinks are weak. As an aspect of diurnal variation, both CO_2 and CH_4 peaked in the morning (08:00 LT for ΔCO_2; 10:00 LT for ΔCH_4), reached local minima in mid-afternoon with increasing PBL height, and increased again in the late afternoon. The lag time in the morning peak between ΔCO_2 and ΔCH_4 might be caused by differing activity schedules of dominant sources such as heating/traffic for ΔCO_2 and waste treatment for ΔCH_4. However, the diurnal variation of the simulated ΔCO_2 and ΔCH_4 from the STILT model showed a different timing of second peak compared to measured values because the STILT model overestimates the afternoon vertical gradient of CO_2, likely linked to estimation of imprecise PBL height.

Although we used a relatively coarse spatial resolution compared to other studies, we identified the contributions of emission sectors over hourly and daily timeframes by combining the model simulation with measured CO_2 and CH_4. Therefore, this approach might provide scientific evidence to support progress toward carbon neutrality, with further improvements expected as higher-resolution of bottom-up inventory and meteorological fields become available.

Acknowledgements This study was supported by the FRIEND (Fine Particle Research Initiative in East Asia Considering National Differences) project through the National Research Foundation of Korea (No. 2023M3G1A109066421) and by the Hankuk University of Foreign Studies Research Fund of 2025. We thank Professor Meehye Lee of Korea University, Dr. Samuel Kenea of the National Institute of Meteorological Sciences (NIMS), and Hyungmo Kang of HUFS for their supports. We appreciated the constructive comments from two anonymous reviewers.

Data Availability The data are available upon reasonable request.

Declarations

Conflict of interest The authors declare that they have no conflict of interest.

References

Allan, R.P., Arias, P.A., Berger, S., Canadell, J.G., Cassou, C., Chen, D., Cherchi, A., Connors, S.L., Coppola, E., Cruz, F.A., Diongue-Niang, A., Doblas-Reyes, F.J., Douville, H., Driouech, F., Edwards, T.L., Engelbrecht, F., Eyring, V., Fischer, E., Flato, G.M., Forster, P., Fox-Kemper, B., Fuglestvedt, J.S., Fyfe, J.C., Gillett, N.P., Gomis, M.I., Gulev, S.K., Gutiérrez, J.M., Hamdi, R., Harold, J., Hauser, M., Hawkins, E., Hewitt, H.T., Johansen, T.G., Jones, C., Jones, R.G., Kaufman, D.S., Klimont, Z., Kopp, R.E., Koven, C., Krinner, G., Lee, J.-Y., Lorenzoni, I., Marotzke, J., Masson-Delmotte, V., Maycock, T.K., Meinshausen, M., Monteiro, P.M.S., Morelli, A., Naik, V., Notz, D., Otto, F., Palmer, M.D., Pinto, I., Pirani, A., Plattner, G.-K., Raghavan, K., Ranasinghe, R., Rogelj, J., Rojas, M., Ruane, A.C., Sallée, J.-B., Samset, B.H., Seneviratne, S.I., Sillmann, J., Sörensson, A.A., Stephenson, T.S., Storelvmo, T., Szopa, S., Thorne, P.W., Trewin, B., Vautard, R., Vera, C., Yassaa, N., Zaehle, S., Zhai, P., Zhang, X., Zickfeld, K.: Summary for policymakers. In: Climate

change 2021: The physical science basis. Contribution of Working Group I to the Sixth Assessment Report of the Intergovernmental Panel on Climate Change. Cambridge University Press, pp. 3–32 (2023). https://doi.org/10.1017/9781009157896.001

Ammoura, L., Xueref-Remy, I., Vogel, F., Gros, V., Baudic, A., Bonsang, B., Delmotte, M., Té, Y., Chevallier, F.: Exploiting stagnant conditions to derive robust emission ratio estimates for CO2, CO and volatile organic compounds in Paris. Atmos. Chem. Phys. **16**, 15653–15664 (2016). https://doi.org/10.5194/acp-16-15653-2016

Baer, D.S., Paul, J.B., Gupta, M., O'keefe, A.: Sensitive absorption measurements in the near-infrared region using off-axis integrated-cavity-output spectroscopy. Appl. Phys. B **75**, 261–265 (2002)

Bezyk, Y., Sówka, I., Górka, M., Nęcki, J.: Spatial and temporal patterns of methane uptake in the urban environment. Urban. Clim. **41**, 101073 (2022)

Bezyk, Y., Dorodnikov, M., Górka, M., Sówka, I., Sawiński, T.: Temperature and soil moisture control CO2 flux and CH4 oxidation in urban ecosystems. Geochemistry **83**, 125989 (2023). https://doi.org/10.1016/j.chemer.2023.125989

Boon, A., Broquet, G., Clifford, D.J., Chevallier, F., Butterfield, D.M., Pison, I., Ramonet, M., Paris, J.D., Ciais, P.: Analysis of the potential of near-ground measurements of CO2 and CH4 in London, UK, for the monitoring of city-scale emissions using an atmospheric transport model. Atmos. Chem. Phys. **16**, 6735–6756 (2016). https://doi.org/10.5194/acp-16-6735-2016

Callewaert, S., Brioude, J., Langerock, B., Duflot, V., Fonteyn, D., Müller, J.F., Metzger, J.M., Hermans, C., Kumps, N., Ramonet, M., Lopez, M., Mahieu, E., De Mazière, M.: Analysis of CO2, CH4, and CO surface and column concentrations observed at Réunion Island by assessing WRF-Chem simulations. Atmos. Chem. Phys. **22**, 7763–7792 (2022). https://doi.org/10.5194/acp-22-7763-2022

Chandra, N., Venkataramani, S., Lal, S., Patra, P.K., Ramonet, M., Lin, X., Sharma, S.K.: Observational evidence of high methane emissions over a city in western India. Atmos. Environ. **202**, 41–52 (2019). https://doi.org/10.1016/j.atmosenv.2019.01.007

Chandra, N., Patra, P.K., Niwa, Y., Ito, A., Iida, Y., Goto, D., Morimoto, S., Kondo, M., Takigawa, M., Hajima, T., Watanabe, M.: Estimated regional CO2 flux and uncertainty based on an ensemble of atmospheric CO2 inversions. Atmos. Chem. Phys. **22**, 9215–9243 (2022). https://doi.org/10.5194/acp-22-9215-2022

Chen, Y., Li, H., Lu, L.: Methane emissions from industrial wastewater treatment systems decoupling from industrial growth in China over the past two decades. NPJ Clim. Atmos. Sci. **8**, 181 (2025). https://doi.org/10.1038/s41612-025-01074-0

Cheng, X.L., Liu, X.M., Liu, Y.J., Hu, F.: Characteristics of CO2 concentration and flux in the Beijing urban area. J. Geophys. Res. Atmos **123**, 1785–1801 (2018). https://doi.org/10.1002/2017JD027409

Choi, Y., Kanaya, Y., Park, S.M., Matsuki, A., Sadanaga, Y., Kim, S.W., Uno, I., Pan, X., Lee, M., Kim, H., Jung, D.H.: Regional variability in black carbon and carbon monoxide ratio from long-term observations over East Asia: assessment of representativeness for black carbon (BC) and carbon monoxide (CO) emission inventories. Atmos. Chem. Phys. **20**, 83–98 (2020). https://doi.org/10.5194/acp-20-83-2020

Choi, Y., Kanaya, Y., Takashima, H., Irie, H., Park, K., Chong, J.: Long-term variation in the tropospheric nitrogen dioxide vertical column density over Korea and Japan from the MAX-DOAS network, 2007–2017. Remote Sens. **13**, 1937 (2021)

Crawford, J.H., Travis, K.R., Judd, L.M., Lefer, B.L., Dibb, J.E., Kim, J., Park, R., Lee, G., Chang, L., Simpas, J.B.B., Cambaliza, M.O.L., Macatangay, R.C., Surapipith, V., Thongboonchoo, N., Oanh, N.T.K., Hien, T.T., Ly, B.T., Salam, A., Ghude, S.D., Latif, M.T., Yu, L.E., Tanimoto, H., Kanaya, Y.: The airborne and satellite investigation of asian air quality (Asia-Aq): An opportunity for international collaboration. In: IGARSS 2022 - 2022 IEEE International geoscience and remote sensing symposium, pp. 6506–6509 (2022)

Crippa, M., Guizzardi, D., Pagani, F., Schiavina, M., Melchiorri, M., Pisoni, E., Graziosi, F., Muntean, M., Maes, J., Dijkstra, L., Van Damme, M., Clarisse, L., Coheur, P.: Insights into the spatial distribution of global, national, and subnational greenhouse gas emissions in the Emissions Database for Global Atmospheric Research (EDGAR v8.0). Earth Syst. Sci. Data **16**, 2811–2830 (2024). https://doi.org/10.5194/essd-16-2811-2024

Dlugokencky, E.J., Myers, R.C., Lang, P.M., Masarie, K.A., Crotwell, A.M., Thoning, K.W., Hall, B.D., Elkins, J.W., Steele, L.P.: Conversion of NOAA atmospheric dry air CH4 mole fractions to a gravimetrically prepared standard scale. J. Geophys. Res **110**, D18306 (2005). https://doi.org/10.1029/2005JD006035

Fasoli, B., Lin, J.C., Bowling, D.R., Mitchell, L., Mendoza, D.: Simulating atmospheric tracer concentrations for spatially distributed receptors: updates to the stochastic time-inverted Lagrangian transport model's R interface (STILT-R version 2). Geosci. Model Dev. **11**, 2813–2824 (2018). https://doi.org/10.5194/gmd-11-2813-2018

Forster, P., Ramaswamy, V., Artaxo, P., Berntsen, T., Betts, R., Fahey, D.W., Haywood, J., Lean, J., Lowe, D.C., Myhre, G., Nganga, J., Prinn, R., Raga, G., Schulz, M., Van Dorland, R.: Changes in atmospheric constituents and in radiative forcing. In: Solomon, S., Qin, D., Manning, M., Chen, Z., Marquis, M., Averyt, K.B., Tignor, M., Miller, H.L. (eds.) Climate change 2007: The physical science basis. Contribution of Working Group I to the Fourth Assessment Report of the Intergovernmental Panel on Climate Change. Cambridge University Press, Cambridge, United Kingdom and New York, NY, USA (2007)

Hall, B.D., Crotwell, A.M., Kitzis, D.R., Mefford, T., Miller, B.R., Schibig, M.F., Tans, P.P.: Revision of the world meteorological organization global atmosphere watch (WMO/GAW) CO2 calibration scale. Atmos. Meas. Tech. **14**, 3015–3032 (2021). https://doi.org/10.5194/amt-14-3015-2021

Kenea, S.T., Lee, H., Joo, S., Li, S., Labzovskii, L.D., Chung, C.-Y., Kim, Y.-H.: Interannual variability of atmospheric CH4 and its driver over South Korea captured by integrated data in 2019. Remote Sens. **13**, 2266 (2021)

Kenea, S.T., Lee, H., Patra, P.K., Li, S., Labzovskii, L.D., Joo, S.: Long-term changes in CH4 emissions: comparing ΔCH4/ΔCO2 ratios between observation and proved model in East Asia (2010–2020). Atmos. Environ. **293**, 119437 (2023). https://doi.org/10.1016/j.atmosenv.2022.119437

Kim, S.-Y., Lee, S.-D., Lee, J.-B., Kim, D.-R., Han, J.-S., Choi, K.-H., Song, C.-K.: Analysis of long-range transport of carbon dioxide and its high concentration events over East Asian region using GOSAT data and GEOS-Chem modeling. Adv. Meteorol. **2015**, 680264 (2015). https://doi.org/10.1155/2015/680264

Kim, J., Jang, J.-A., Oh, Y.-S., Lee, H., Joo, S., Kim, S., Boo, K.-O., Lee, Y.G.: Anthropogenic carbon dioxide origin tracing study in Anmyeon-do, South Korea: Based on STILT-footprint and emissions data. Sci. Total. Environ. **894**, 164677 (2023). https://doi.org/10.1016/j.scitotenv.2023.164677

KMA.: Report of global atmosphere watch 2024.In: Korea meteorological administration, pp. 99–102 (2025). Accessed 20 Dec 2025

Kort, E.A., Angevine, W.M., Duren, R., Miller, C.E.: Surface observations for monitoring urban fossil fuel CO2 emissions: minimum site location requirements for the Los Angeles megacity. J. Geophys. Res. Atmos. **118**, 1577–1584 (2013)

Lan, X., Tans, P., Thoning, K.W.: Trends in globally-averaged CO2 determined from NOAA Global Monitoring Laboratory measurements. Version Friday, 05-Sep-2025 12:12:59 MDT https://doi.org/10.15138/9N0H-ZH07. Accessed Aug 18th 2025

Lan, X., Thoning, K.W., Dlugokencky, E.J.: Trends in globally-averaged CH4, N2O, and SF6 determined from NOAA Global Monitoring Laboratory measurements. Version 2025–09, https://doi.org/10.15138/P8XG-AA10. Accessed Aug 18th 2025

Lee, H., Han, S.-O., Ryoo, S.-B., Lee, J.-S., Lee, G.-W.: The measurement of atmospheric CO2 at KMA GAW regional stations, its characteristics, and comparisons with other East Asian sites. Atmos. Chem. Phys. **19**, 2149–2163 (2019)

Lee, H., Dlugokencky, E.J., Turnbull, J.C., Lee, S., Lehman, S.J., Miller, J.B., Pétron, G., Lim, J.-S., Lee, G.-W., Lee, S.-S.: Observations of atmospheric 14 CO2 at Anmyeondo GAW station, South Korea: implications for fossil fuel CO2 and emission ratios. Atmos. Chem. Phys. **20**, 12033–12045 (2020)

Li, S., Kenea, S.T., Kim, S., Yoo, H.-J., Joo, S., Lee, H., Oh, S., Jeong, M.J., Seo, W., Ko, M., Lee, S., Oh, Y.-S., Shin, D.: Latitudinal distribution and sources analysis of greenhouse gases and air pollutants observed during the 2021 Yellow Sea Air Quality campaign aboard a research vessel. Atmos. Environ. **317**, 120201 (2024). https://doi.org/10.1016/j.atmosenv.2023.120201

Lin, J.C., Gerbig, C., Wofsy, S.C., Andrews, A.E., Daube, B.C., Davis, K.J., Grainger, C.A.: A near-field tool for simulating the upstream influence of atmospheric observations: The stochastic time-inverted lagrangian transport (STILT) model. J. Geophys. Res.: Atmos. **108**, 4493 (2003). https://doi.org/10.1029/2002JD003161

Maier, F., Gerbig, C., Levin, I., Super, I., Marshall, J., Hammer, S.: Effects of point source emission heights in WRF–STILT: a step towards exploiting nocturnal observations in models. Geosci. Model Dev. Discuss **2021**, 1–25 (2021)

Masson-Delmotte, V.P., Zhai, A., Pirani, S., Connors, C., Péan, S., Berger, N., Caud, Y., Chen, L., Goldfarb, M., Gomis, M., Huang, K., Leitzell, E., Lonnoy, J., Matthews, T., Maycock, T., Waterfield, O., Yelekci, R.Y., Zhou, B.E.: IPCC, 2021: Climate change 2021: The physical science basis. In: Contribution of Working Group I to the Sixth Assessment Report of the Intergovernmental Panel on Climate Change, Cambridge University Press, Cambridge, United Kingdom and New York, NY, USA (2021)

McKain, K., Wofsy, S.C., Nehrkorn, T., Eluszkiewicz, J., Ehleringer, J.R., Stephens, B.B.: Assessment of ground-based atmospheric observations for verification of greenhouse gas emissions from an urban region. Proc. Natl. Acad. Sci. u. s. a. **109**, 8423–8428 (2012). https://doi.org/10.1073/pnas.1116645109

McKain, K., Down, A., Raciti, S.M., Budney, J., Hutyra, L.R., Floerchinger, C., Herndon, S.C., Nehrkorn, T., Zahniser, M.S., Jackson, R.B., Phillips, N., Wofsy, S.C.: Methane emissions from natural gas infrastructure and use in the urban region of Boston, Massachusetts. Proc. Natl. Acad. Sci **112**, 1941–1946 (2015)

Miller, S.M., Wofsy, S.C., Michalak, A.M., Kort, E.A., Andrews, A.E., Biraud, S.C., Dlugokencky, E.J., Eluszkiewicz, J., Fischer, M.L., Janssens-Maenhout, G.: Anthropogenic emissions of methane in the United States. Proc. Natl. Acad. Sci. u. s. a. **110**, 20018–20022 (2013)

Moon, J., Shim, C., Seo, J., Han, J.: Evaluation of Korean methane emission sources with satellite retrievals by spatial correlation analysis. Environ. Monit. Assess **196**, 296 (2024). https://doi.org/10.1007/s10661-024-12449-w

Nara, H., Tanimoto, H., Tohjima, Y., Mukai, H., Nojiri, Y., Machida, T.: Emissions of methane from offshore oil and gas platforms in Southeast Asia. Sci. Rep. **4**, 6503 (2014). https://doi.org/10.1038/srep06503

Nehrkorn, T., Eluszkiewicz, J., Wofsy, S.C., Lin, J.C., Gerbig, C., Longo, M., Freitas, S.: Coupled weather research and forecasting–stochastic time-inverted lagrangian transport (WRF–STILT) model. Meteorol. Atmos. Phys. **107**, 51–64 (2010)

Park, C., Jeong, S., Shin, Y.-S., Cha, Y.-S., Lee, H.-C.: Reduction in urban atmospheric CO2 enhancement in Seoul, South Korea, resulting from social distancing policies during the COVID-19 pandemic. Atmos. Pollut. Res **12**, 101176 (2021)

Park, H., Jeong, S., Park, H., Kim, Y., Park, C., Sim, S., Kim, J., Park, J., Kim, H., Choi, J.: Unexpected urban methane hotspots captured from aircraft observations. ACS Earth Space Chem. **6**, 755–765 (2022). https://doi.org/10.1021/acsearthspacechem.1c00431

Parry, M.L.: 2007: Climate change 2007-impacts. In: adaptation and vulnerability: Working group II contribution to the fourth assessment report of the IPCC. Cambridge University Press (2007)

Paul, J.B., Lapson, L., Anderson, J.G.: Ultrasensitive absorption spectroscopy with a high-finesse optical cavity and off-axis alignment. Appl. Opt. **40**, 4904–4910 (2001)

Rigby, M., Prinn, R.G., Fraser, P.J., Simmonds, P.G., Langenfelds, R.L., Huang, J., Cunnold, D.M., Steele, L.P., Krummel, P.B., Weiss, R.F.: Renewed growth of atmospheric methane. Geophys. Res. Lett. **35**, L22805 (2008). https://doi.org/10.1029/2008GL036037

Sargent, M., Barrera, Y., Nehrkorn, T., Hutyra, L.R., Gately, C.K., Jones, T., McKain, K., Sweeney, C., Hegarty, J., Hardiman, B., Wang, J.A., Wofsy, S.C.: Anthropogenic and biogenic CO(2) fluxes in the Boston urban region. Proc. Natl. Acad. Sci. U. S. A. **115**, 7491–7496 (2018). https://doi.org/10.1073/pnas.1803715115

Seto, K.C., S. Dhakal, A. Bigio, H. Blanco, G.C. Delgado, D. Dewar, L. Huang, A. Inaba, A. Kansal, S. Lwasa, J.E. McMahon, D.B. Müller, J. Murakami, H. Nagendra and A. Ramaswami: Human settlements, infrastructure and spatial planning. In O. Edenhofer, R. Pichs-Madruga, Y. Sokona, E. Farahani, S. Kadner, K. Seyboth, A. Adler, I. Baum, S. Brunner, P. Eickemeier, B. Kriemann, J. Savolainen, S. Schlömer, C. Stechow, T. Zwickel and J.C. Minx (eds.), Climate change 2014: mitigation of climate change. Contribution of Working Group III to the fifth assessment report of the Intergovernmental Panel on Climate Change, Cambridge University Press, Cambridge and New York, NY. (2014)

Shim, C., Han, J., Henze, D.K., Yoon, T.: Identifying local anthropogenic CO2 emissions with satellite retrievals: A case study in South Korea. Int. J. Remote Sens. **40**, 1011–1029 (2019). https://doi.org/10.1080/01431161.2018.1523585

Sim, S., Lee, H., Oh, E., Kim, S., Ciais, P., Piao, S., Lin, J.C., Mallia, D.V., Lee, S., Kim, Y.-H.: Short-term reduction of regional enhancement of atmospheric CO2 in China during the first COVID-19 pandemic period. Environ. Res. Lett. **17**, 024036 (2022)

Solazzo, E., Crippa, M., Guizzardi, D., Muntean, M., Choulga, M., Janssens-Maenhout, G.: Uncertainties in the emissions database for global atmospheric research (EDGAR) emission inventory of greenhouse gases. Atmos. Chem. Phys. **21**, 5655–5683 (2021). https://doi.org/10.5194/acp-21-5655-2021

Soleimanpour, M., Alizadeh, O., Sabetghadam, S.: Analysis of diurnal to seasonal variations and trends in air pollution potential in an urban area. Sci. Rep. **13**, 21065 (2023). https://doi.org/10.1038/s41598-023-48420-x

Sreenivas, G., Mahesh, P., Subin, J., Kanchana, A.L., Rao, P.V.N., Dadhwal, V.K.: Influence of meteorology and interrelationship with greenhouse gases (CO2 and CH4) at a suburban site of India. Atmos. Chem. Phys. **16**, 3953–3967 (2016). https://doi.org/10.5194/acp-16-3953-2016

Sreenivas, G., Mahesh, P., Mahalakshmi, D.V., Kanchana, A.L., Chandra, N., Patra, P.K., Raja, P., SeshaSai, M.V.R., Sripada, S., Rao, P.V.N., Dadhwal, V.K.: Seasonal and annual variations of CO2 and CH4 at Shadnagar, a semi-urban site. Sci. Total Environ. **819**, 153114 (2022). https://doi.org/10.1016/j.scitotenv.2022.153114

Stocker, T., Qin, D., Platner, G.-K.: Climate change 2013: The physical science basis. In: Contribution of Working Group I to the Fifth Assessment Report of the Intergovernmental Panel on Climate

Change, edited by: Intergovernmental Panel on Climate Change, Cambridge University Press, Cambridge (2013)

Tohjima, Y., Kubo, M., Minejima, C., Mukai, H., Tanimoto, H., Ganshin, A., Maksyutov, S., Katsumata, K., Machida, T., Kita, K.: Temporal changes in the emissions of CH4 and CO from China estimated from CH4/CO2 and CO/CO2 correlations observed at Hateruma Island. Atmos. Chem. Phys. **14**, 1663–1677 (2014). https://doi.org/10.5194/acp-14-1663-2014

UNFCCC.: Paris agreement. United Nations Framework Convention on Climate Change, FCCC/CP/2015/L.9/Rev.1 (2015). Available at: https://unfccc.int/sites/default/files/english_paris_agreement.pdf

Wei, C., Wang, M., Fu, Q., Dai, C., Huang, R., Bao, Q.: Temporal characteristics of greenhouse gases (CO2 and CH4) in the megacity Shanghai, China: association with air pollutants and meteorological conditions. Atmos. Res. **235**, 104759 (2020)

Xia, L., Zhang, G., Zhan, M., Li, B., Kong, P.: Seasonal variations of atmospheric CH4 at Jingdezhen station in Central China: understanding the regional transport and its correlation with CO2 and CO. Atmos. Res. **241**, 104982 (2020)

Yang, H., Wu, K., Wang, T., Wang, P., Zhou, M.: Atmospheric anthropogenic CO2 variations observed by tower in-situ measurements and simulated by the STILT model in the Beijing megacity region. Atmos. Res. **325**, 108258 (2025). https://doi.org/10.1016/j.atmosres.2025.108258